

TiO₂ Nanotube Arrays Annealed in N₂ for Efficient Lithium-Ion Intercalation

Dawei Liu,[†] Peng Xiao,^{†,‡} Yunhuai Zhang,^{†,§} Betzaida B. Garcia,[†] Qifeng Zhang,[†] Qing Guo,^{||} Richard Champion,[⊥] and Guozhong Cao^{*,†}

Department of Materials Science and Engineering, University of Washington, Seattle, Washington, Department of Physics, Department of Chemical Engineering, Chongqing University, People's Republic of China, Department of Mechanical Engineering, and Department of Chemical Engineering, University of Washington, Seattle, Washington

Received: February 13, 2008; Revised Manuscript Received: April 2, 2008

Anatase titania nanotube arrays were fabricated by means of anodization and annealed at 300, 400, and 500 °C in N₂. Lithium-ion intercalation measurements revealed that annealing in nitrogen resulted in much enhanced lithium-ion insertion capacity and improved cyclic stability. TiO₂ nanotube arrays annealed at 300 °C exhibited the best lithium-ion intercalation property with an initial high discharge capacity up to 240 mA·h/g at a high current density of 320 mA/g. The excellent discharge capacity at a high charge/discharge rate could be attributed to the large surface area of the nanotube arrays and a short facile diffusion path for lithium-ion intercalation as well as improved electrical conductivity. As the annealing temperature increased, the discharge capacity decreased, but the cyclic stability improved; 400 °C annealed TiO₂ nanotube arrays possessed an initial discharge capacity of 163 mA·h/g and retained 145 mA·h/g at the 50th cycle. The relationship between the annealing conditions, microstructure, and lithium-ion intercalation properties of TiO₂ nanotube arrays was discussed.

1. Introduction

Titanium dioxide has been investigated as a favorable candidate for energy conversion and storage applications due to its low cost, abundance in nature, and chemical stability.^{1,2} For example, mesoporous anatase titania has been studied intensively in the past decades as a wide band gap semiconductor electrode for low-cost dye-sensitized solar cells.^{3,4} TiO₂ has been researched as a photocatalyst^{5,6} and as electrochromic devices.^{7,8} Recently both anatase and rutile TiO₂ have also been studied as an intercalation host in lithium-ion batteries.^{9–12}

As lithium-ion batteries are becoming more and more popular and in use daily, the traditional anode of graphite in lithium-ion batteries is now facing a big challenge to its service as the safety issues incurred during its cycling are becoming more and more serious. The potential for lithium intercalation into anode graphite is close to that of the Li⁺/Li redox couple, leading to the possibility of lithium plating during charge which may cause an explosion if exposed to air.¹³ For this reason, an alternative to graphite as the new anode of lithium-ion batteries is now being actively searched. In comparison to other possible anode compounds such as CoO and SnO₂,^{14,15} TiO₂ has the advantage of safe lithium-ion intercalation voltage and relatively stable cycle performance.¹⁶ Thus, it is regarded as an excellent substitute for graphite as the anode. However, since the Li⁺ diffusivity in TiO₂ is very low, the bulk TiO₂ film suffers low lithium-ion storage capacity. So the concern is how to improve the lithium-ion intercalation capacity of TiO₂ so as to be used as the anode in lithium-ion batteries. By sharing the advantages of nanostructures such as shorter length for both electronic and

Li⁺ transport, higher electrode–electrolyte contact area, and better accommodation of the strain of Li⁺ insertion/extraction,^{17,18} nanostructured TiO₂ has exhibited a much better performance than bulk titania;¹⁹ values higher than the theoretical intercalation limit of 0.5 Li per TiO₂, or say a discharge capacity of 168 mA·h/g, have already been observed for hydrothermally fabricated TiO₂ nanotubes.^{20–22} However, the nanotubes grown from the hydrothermal method are random with varied orientations, thus less favoring the electron and lithium-ion transport. Nanotube arrays fabricated by anodization of pristine titanium have the advantage of ordered structure with uniform tube orientation which not only facilitates the close contact between nanotubes and electrolyte but also favors both electron and lithium-ion transport. In addition, in anodization, the structure parameters including tube length, tube diameter, and tube wall thickness are easily controlled by adjusting electrolyte composition, anodization voltage, and time.²³ Nanotube arrays are also favorable for high energy storage since they are compactly ordered with the length of every single tube up to several micrometers. Despite the fact that the as-grown TiO₂ nanotube arrays are amorphous, well-designed post heat treatment can be applied to form desired crystalline structures. This paper reports an experimental study of anatase TiO₂ nanotube arrays annealed at temperatures ranging from 300 to 500 °C in nitrogen and revealed enhanced lithium-ion intercalation properties and improved cyclic stability.

2. Experimental Section

Titania nanotube arrays were synthesized by an anodic oxidation method according to the literature.²³ In brief, titanium foil (99.94%) of 0.5 mm thickness was chemically etched in 30% HCl solution at approximately 80 °C for about 20 min. After rinsing thoroughly with DI water, the clean titanium foil was anodized in the electrolyte of 0.1 M KF and 1.0 M NaHSO₄ with a platinum foil as counter electrode at a constant potential of 20 V at room temperature for 1 h. The as-grown titania

* To whom correspondence should be addressed. E-mail: gzc@u.washington.edu.

[†] Department of Materials Science and Engineering, University of Washington.

[‡] Department of Physics, Chongqing University.

[§] Department of Chemical Engineering, Chongqing University.

^{||} Department of Mechanical Engineering, University of Washington.

[⊥] Department of Chemical Engineering, University of Washington.

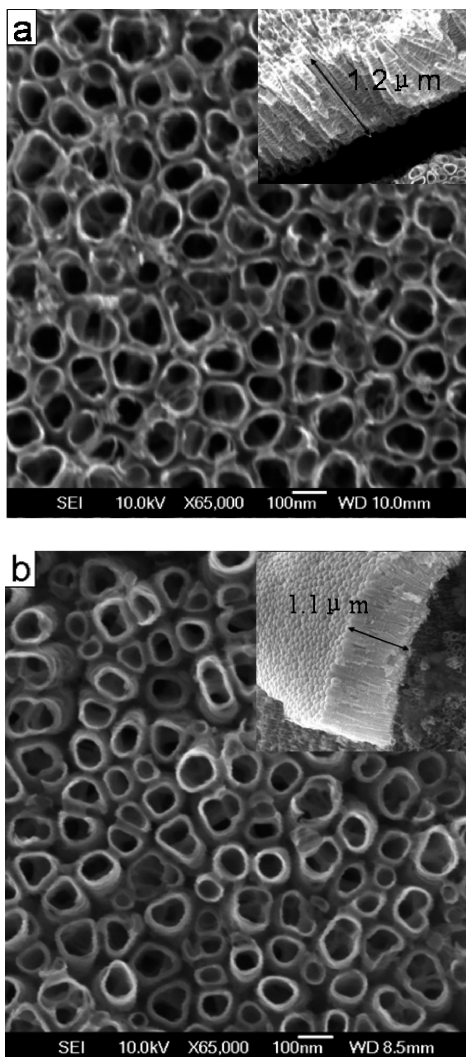


Figure 1. SEM images of (a) as-grown amorphous titania nanotube arrays and (b) anatase titania nanotube arrays annealed at 300 °C in nitrogen for 3 h.

nanotube arrays were calcined at temperatures of 300, 400, and 500 °C under a dry N₂ gas flow with a heating rate of 4 °C/min and dwelled at the maximum temperature for 3 h. Then X-ray diffraction (XRD, Philips 1820 X-ray diffractometer) and scanning electron microscopy (SEM, Philips, JEOL JSM7000) were carried out to characterize the crystallization state and morphology. Electrochemical properties of TiO₂ nanotube arrays were investigated using a standard three-electrode system, with 1 M LiClO₄ in propylene carbonate (PC) as the electrolyte, a Pt mesh as the counter electrode, and Ag/AgCl as the reference electrode. Cyclic voltammetric (CV) tests were conducted between -0.2 and -2.2 V with a scan rate of 5 mV/s; chronopotentiometric (CP) tests were carried out in the voltage range from -0.6 to -2.1 V with a constant current density of 320 mA/g. Both the CVs and CPs were done by using an electrochemical analyzer (CH Instruments, model 605B).

3. Results and Discussion

Figure 1 compares the typical SEM images of the TiO₂ nanotube arrays before (Figure 1a) and after (Figure 1b) calcination at 300 °C in N₂ for 3 h. Before calcination, the inner diameter of TiO₂ nanotubes was approximately of 100 nm, and wall thickness was ~10 nm. After being calcined for 3 h, the inner diameter decreased to ~90 nm, and the wall thickness

increased to ~15 nm. The length of TiO₂ nanotube arrays underwent shrinkage, from ~1.2 to 1.1 μm. Similar morphologies were observed for TiO₂ nanotube arrays annealed at 400 and 500 °C, except that the inner diameters decreased further (to respective ~85 and 78 nm) and the wall thickness increased further (to respective ~17 and 20 nm) with more shrinkage in length (to respective ~1.05 and 1.0 μm). The same morphology change was also reported in the literature when TiO₂ nanotubes were annealed in Ar.²⁴ XRD revealed that the as-grown TiO₂ nanotube arrays were amorphous without any detectable crystalline phase; however, anatase phase was confirmed in all TiO₂ nanotube arrays annealed in 300, 400, and 500 °C in nitrogen for 3 h. No rutile phase was detected, and no peak broadening could be meaningfully determined, though it was expected that a higher annealing temperature would result in better crystallinity.

Figure 2 shows the initial cyclic voltammograms of as-grown and annealed TiO₂ nanotube arrays tested under the identical conditions and reveals some significant differences in lithium-ion intercalation properties between the as-grown and annealed arrays. The as-grown TiO₂ nanotube arrays were amorphous and showed neither a cathodic nor an anodic peak throughout the entire voltage scan range (Figure 2a). Such a CV curve suggests no phase transition occurred at a given voltage. However, lithium-ion intercalation and deintercalation peaks were observed in all three annealed samples with varied peak intensities. From the CV curve of the 300 °C annealed TiO₂ nanotube arrays (Figure 2b), one broad cathodic peak centered at -1.95 V was identified and one weak anodic peak at -1.45 V was also observed. This set of cathodic and anodic peaks was ascribed to lithium-ion intercalation and deintercalation and has been considered as the characteristic peaks of anatase TiO₂ in the literature.²⁵ It should also be noted that the absence of symmetry in the CV curve here reveals the difference in lithium-ion insertion and extraction capabilities. Under the same scan rate, more lithium ions were inserted into the TiO₂ lattice, but only a portion of the inserted lithium ions were extracted in the negative scan. The CV curves of TiO₂ nanotube arrays annealed at 400 and 500 °C (Figure 2, parts c and d) revealed also the characteristic peaks of lithium-ion intercalation and deintercalation with much improved symmetry, suggesting comparable capabilities of lithium-ion intercalation to and deintercalation from the TiO₂ nanotube arrays. As mentioned earlier, it is anticipated that the higher annealing temperature would improve the crystallinity of anatase titania; however, experimental verification of the improved crystallinity is still underway.

In Figure 3 are the initial CP lithium-ion intercalation and deintercalation curves of as-grown and annealed TiO₂ nanotube arrays with a current density of 320 mA/g. As one would expect based on the CV curves discussed above, there are noticeable differences among those four CP curves. The discharge capacity varies more than 50%, and the shapes of the curves are different. For the as-grown amorphous TiO₂ nanotube arrays (Figure 3a), there were no plateaus in both the charge and discharge curves, agreeing very well with there being no detectable cathodic and anodic peaks in the CV curve. This type of discharge and charge curve was reported in the literature²⁶ and was described as a single-phase process during lithium-ion intercalation, which was an indication of poor crystallinity.²⁷ It is also noted that after the completion of one cycle of lithium-ion intercalation and deintercalation, the curve of TiO₂ nanotube arrays did not return to its starting point and there was a capacity loss of almost 70 mA·h/g. Figure 3b is the CP curve of 300 °C annealed nanotube arrays, and the highest discharge capacity of 240 mA·h/g

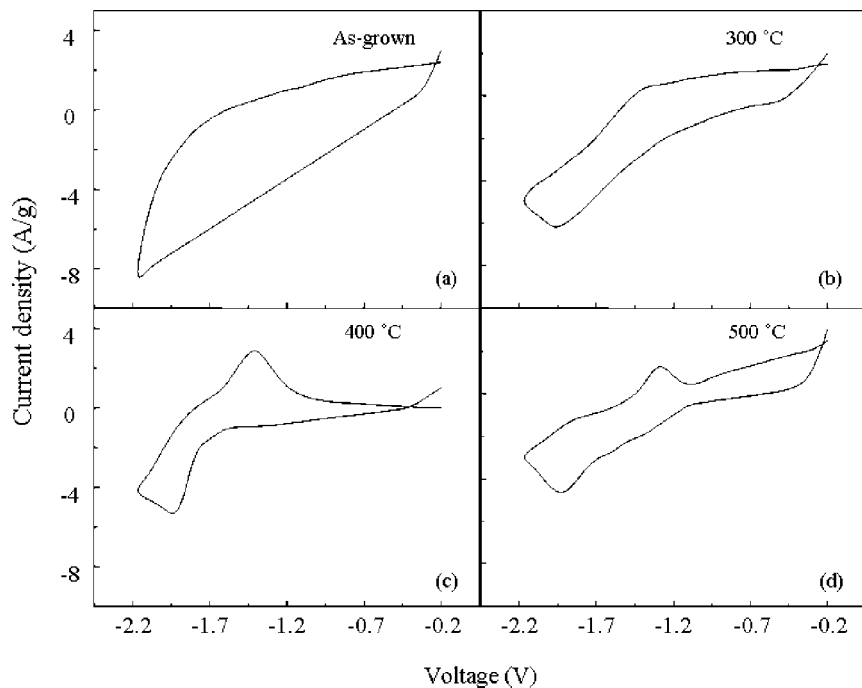


Figure 2. Cyclic voltammograms of titania nanotube arrays in 1 M LiClO₄ in propylene carbonate with a scan rate of 5 mV/s in a voltage range between -0.2 and -2.2 V: (a) as-grown amorphous TiO₂ nanotube arrays, (b) anatase TiO₂ nanotube arrays annealed at 300, (c) 400, and (d) at 500 °C in nitrogen for 3 h.

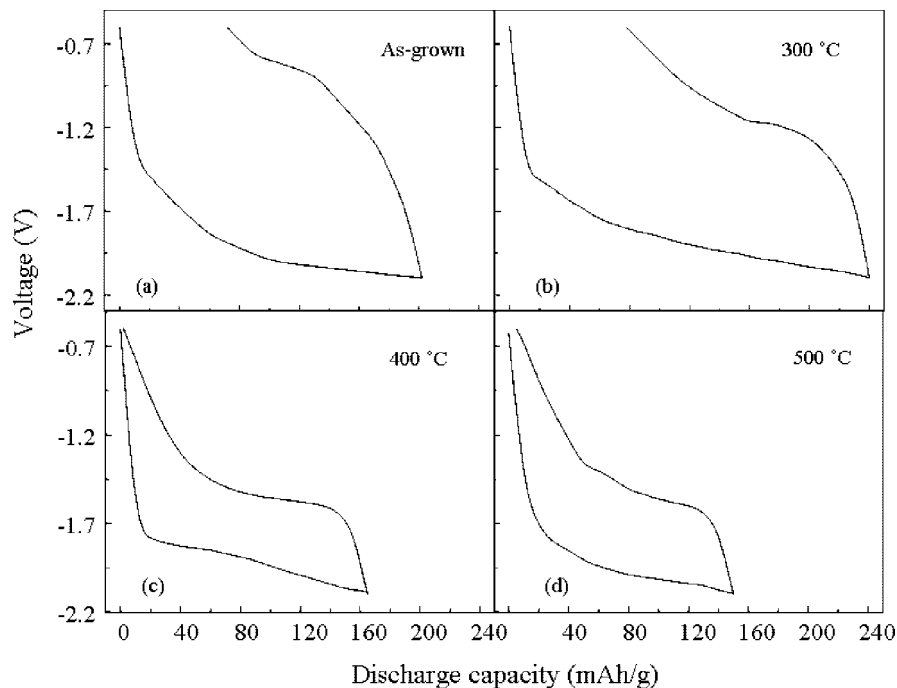


Figure 3. Chronopotentiometric charge/discharge curves in the first cycle at a current density 320 mA·h/g of (a) as-grown amorphous TiO₂ nanotube arrays and (b) anatase TiO₂ nanotube arrays annealed at 300, (c) 400, and (d) 500 °C in nitrogen for 3 h.

was obtained in the first cycle. However, the charge capacity was only 167 mA·h/g, about 70% of the initial discharge capacity, revealing a poor reversibility. Similar irreversible capacity was also reported in hydrothermally grown TiO₂ nanotube electrodes which were annealed in O₂ at 350 °C and was ascribed to the surface defects that resulted in a certain fraction of lithium ions being trapped in the imperfection, which could not be extracted.²¹ The CP curve of 400 °C annealed TiO₂ nanotube arrays (Figure 3c) revealed a noticeable plateau in the discharge curve in a voltage range between -1.8 and -1.9 V, agreeing very well with the

position of the cathodic peak in Figure 2c. Most lithium ions were intercalated into the anatase TiO₂ structure, resulting in a phase transition from TiO₂ to lithiated TiO₂. The charge (deintercalation) plateau was observed at a voltage ranging from -1.6 to -1.5 V, indicating the reverse phase transition from lithiated TiO₂ to anatase TiO₂. The discharge (163 mA·h/g) and charge (162 mA·h/g) capacities were almost identical, revealing its good reversibility. A reduced discharge capacity than that of the 300 °C annealed sample could be attributed to the absence of the previously mentioned “crystal imperfection” which was accountable for the irreversible

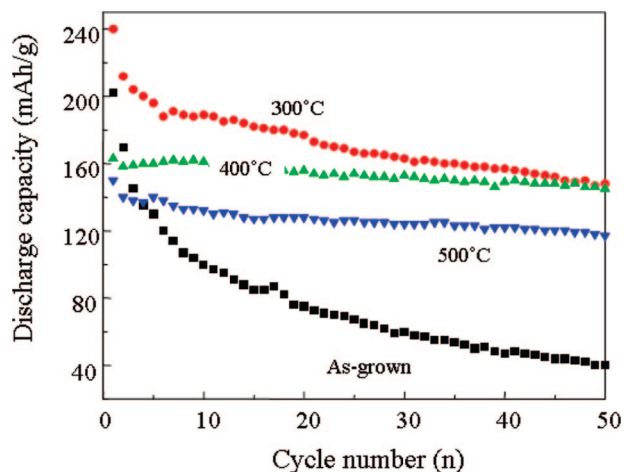


Figure 4. Li⁺-ion intercalation discharge capacity of amorphous as-grown TiO₂ nanotube arrays and anatase TiO₂ nanotube arrays annealed at 300, 400, and 500 °C in nitrogen for 3 h as a function of cyclic numbers. The measurements were carried out in a potential window between -0.6 and -2.1 V vs Ag/AgCl as a reference electrode at a current density of 320 mA/g.

capacities in the 300 °C arrays. The CP curve of 500 °C annealed TiO₂ nanotube arrays (Figure 3d) was found to be similar to that of the 400 °C annealed sample with nearly as good reversibility but smaller discharge and charge capacities of 150 and 145 mA·h/g, respectively.

The cyclic stability of the as-grown and annealed TiO₂ nanotube arrays for lithium-ion intercalation was measured by a CP test for 50 continuous charge/discharge cycles with a current density of 320 mA/g. A comparison of the discharge capacities of 300, 400, and 500 °C annealed TiO₂ nanotube arrays together with amorphous as-grown TiO₂ nanotube arrays can be found in Figure 4. For the amorphous as-grown TiO₂ nanotube arrays, the discharge capacity began with an exciting value of 202 mA·h/g. However, the degradation was significant and rapid, and after 50 cycles, the discharge capacity was reduced to merely 40 mA·h/g, approximately 20% of the initial discharge capacity. Such a rapid and substantial loss of discharge capacity is commonly found in amorphous TiO₂ electrodes²⁸ and is at least partially attributable to PC electrolyte decomposition in low intercalation voltages which was often induced by high charge-transfer resistance of the intercalation electrode.²⁹ Figure 5 compares the surface morphology of as-grown TiO₂ and 400 °C annealed TiO₂ nanotube arrays after 50 cycles of charge/discharge measurements; the surface of the as-grown nanotube arrays was covered by a thick carbon-rich film (~1 μm) as revealed by energy-dispersive X-ray (EDX) analyses, which would severely hinder diffusion of lithium ions. The impedance measurement indeed showed a high charge-transfer resistance of the as-grown amorphous TiO₂ arrays; high electrical resistance would result in the development of high electric field on the entrance of the TiO₂ nanotube during charge/discharge processing. Such a high electric field in turn could lead to the electrolyte decomposition, resulting in deposition of organic film on the surface of the TiO₂ nanotube arrays.³⁰ In contrast, no deposition of a film on the surface of all three annealed TiO₂ nanotube arrays was observed, and it is attributed to much reduced charge-transfer resistance (~0.81 × 10⁵ Ω) with the magnitude typically 1/10 of that of the as-grown amorphous TiO₂ nanotube arrays (~7.54 × 10⁵ Ω).³¹ It is also very clear that TiO₂ nanotube arrays annealed at 400 and 500 °C possessed better cyclic stability than that

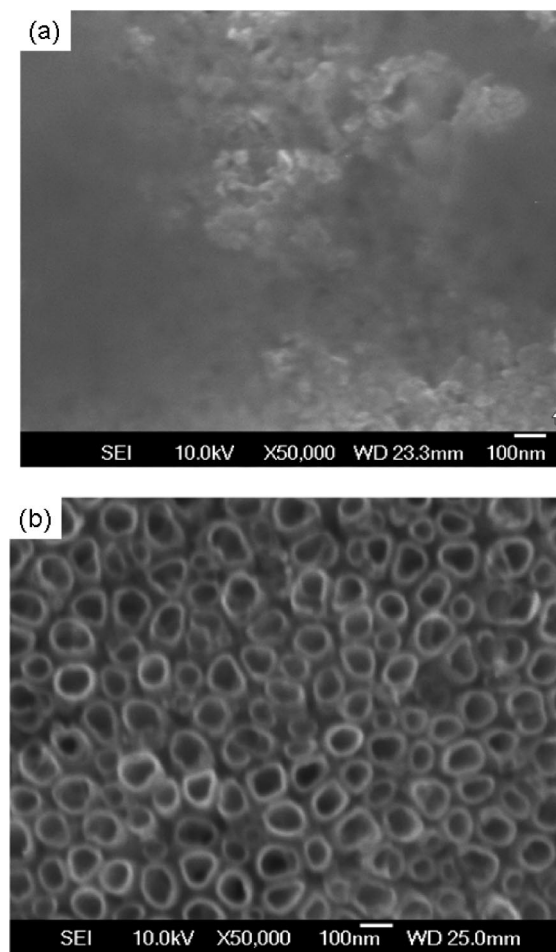


Figure 5. SEM images of (a) as-grown amorphous and (b) 400 °C annealed titania nanotube arrays after 50 cycles of chronopotentiometric charge/discharge measurement at a current density of 320 mA·h/g in the voltage range between -0.6 and -2.1 V.

of 300 °C annealed TiO₂ nanotube arrays. It could be seen that the 300 °C arrays delivered the highest discharge capacity during all the cycling life. Beginning with 240 mA·h/g, it dropped to 212 mA·h/g in the second cycle and after 50 cycles with a discharge capacity of 148 mA·h/g. The high initial capacity and relatively rapid degradation were associated with the irreversible lithium-ion trapping in the crystal imperfection. Both 400 and 500 °C annealed TiO₂ nanotube arrays showed very good cyclic stability, though the discharge capacity of 400 °C annealed TiO₂ nanotube arrays was always higher than that of the 500 °C annealed sample, beginning with a capacity of 163 mA·h/g, retaining a capacity of 160 mA·h/g at the 10th cycle (i.e., 0.18% decrease per cycle), and 145 mA·h/g at the 50th cycle (a loss of 0.22% per cycle). The 500 °C annealed TiO₂ nanotube arrays had an initial capacity of 150 mA·h/g, and 117 mA·h/g at 50th cycle, with a loss of 0.44% per cycle.

It is not entirely clear what is the exact mechanism(s) leading to lower lithium-ion intercalation capacities of 500 °C annealed TiO₂ nanotube arrays than that of the 400 °C annealed sample; however, such temperature dependence is most likely due to the change of crystallinity and micro- or nanostructures. The crystallinity and particle size are already known to have appreciable impacts on the lithium-ion intercalation properties of vanadium pentoxide.^{32,33} Although XRD spectra did not reveal a detectable change in crystallinity in TiO₂ nanotube arrays annealed under those two

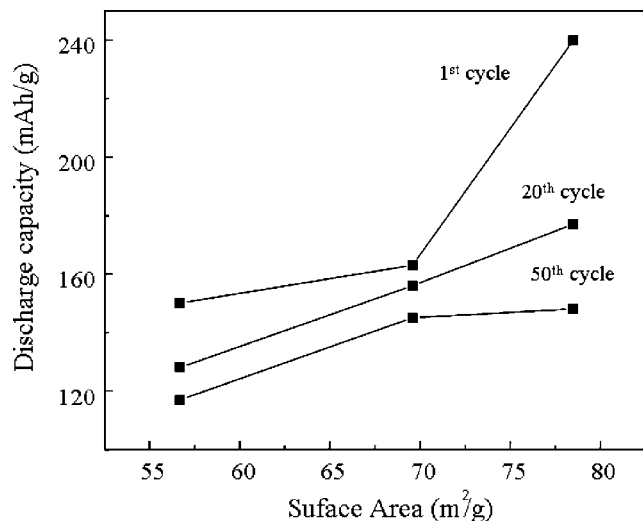


Figure 6. Discharge capacities at 1st, 20th, and 50th cycles of anatase TiO₂ nanotube arrays annealed at 300, 400, and 500 °C in nitrogen for 3 h as a function of their specific surface area. The lines are just to serve as a visual guidance.

temperatures, possible variation in crystallinity cannot be ruled out completely. SEM images also revealed that the wall thickness increased from ~17 to ~20 nm when the annealing temperature increased from 400 to 500 °C. According to the lithiation study for zero-dimension nanoparticles,³⁴ nanosized particles, in the lithium-ion intercalation process, will form a lithium-rich shell of compound, Li₁TiO₂ with a shell thickness of ~4 nm regardless of the particle size. Inside the Li₁TiO₂ shell formed the lithium titanate phase Li_xTiO₂ ($x = 0.55-0.7$ ³⁵) whose fraction increased as the particle size increased. One-dimension nanotube arrays should have a similar intercalation effect, i.e., forming a shell of Li₁TiO₂. Assuming the same shell thickness after full lithiation, the 20 nm wall had a larger ratio of Li_{0.55-0.7}TiO₂/Li₁TiO₂, than the 17 nm wall and, thus, intercalated less total lithium ions. Another possibility is that initial nucleation of rutile phase may occur at 500 °C. Although rutile TiO₂ is capable of lithium-ion intercalation, it has been reported to have a lower intercalation capacity than anatase TiO₂.^{36,37}

The change of diameter and wall thickness with the annealing temperatures may also contribute to the change of lithium-ion intercalation properties as well. SEM images revealed that the diameters of TiO₂ nanotube arrays decreased with an increased annealing temperature, accompanied with increased tube thickness. Assuming there is no appreciable densification at temperatures below 500 °C or the nanotubes are dense, the specific surface area of the TiO₂ nanotube arrays can then be easily calculated. The surface areas of 300, 400, and 500 °C annealed TiO₂ nanotube arrays were estimated to be 78, 70, and 57 m²/g. Figure 6 summarizes the lithium-ion discharge capacities at the 1st, 20th, and 50th cycles, as a function of the specific surface area. There is an obvious general trend of a decrease in discharge capacities with a decreased specific surface area. Since the lithium-ion diffusivity in the lithium-rich phase was very poor,³⁴ the most efficient lithium-ion intercalation would occur near the surface or on the subsurface layer. A decrease in surface area would result in smaller discharge capacities. Further research is required to quantify the dependence of lithium intercalation capacity on the specific surface area when the crystallinity and particle size are kept the same.

4. Conclusions

Anatase TiO₂ nanotube arrays fabricated by anodic oxidation and annealed in nitrogen at temperatures between 300 and 500 °C exhibited very promising lithium-ion intercalation properties. A high initial discharge capacity of 240 mA·h/g was found in 300 °C annealed TiO₂ nanotube arrays, which was partially attributed to the crystal imperfection. A discharge capacity of ~160 mA·h/g was obtained in 400 °C annealed samples with excellent cyclic stability. The improved lithium-ion intercalation capacity and good cycling ability were attributed to the desirable nanostructure: large surface area, short diffusion path, and favorable crystallinity, and also to the reduced charge-transfer resistance after N₂ annealing.

Acknowledgment. This work has been supported in part by the National Science Foundation (DMI-0455994) and the Air Force Office of Scientific Research (AFOSR-MURI, FA9550-06-1-032). Peng Xiao and Yunhuai Zhang gratefully acknowledge the fellowship from the Chinese Scholarship Council.

References and Notes

- Ollis, D. F.; Pellizzetti, E.; Serpone, N. *Environ. Sci. Technol.* **1991**, *25*, 1523.
- Navio, J. A.; Colvin, G.; Herrman, J. M. *J. Photochem. Photobiol., A* **1997**, *108*, 179.
- Gratzel, M. *Nature* **2001**, *414*, 338.
- Chou, T.; Zhang, Q.; Russo, B.; Fryxell, G. E.; Cao, G. Z. *J. Phys. Chem. C* **2007**, *111*, 6296.
- Ohko, Y.; Fujishima, A.; Hashimoto, K. *J. Phys. Chem. B* **1998**, *102*, 2699.
- Mukai, S. R.; Nishihara, H.; Shichi, S.; Tamon, H. *Chem. Mater.* **2004**, *16*, 4987.
- Wang, Z. C.; Hu, X. F. *Electrochim. Acta* **2001**, *46*, 1951.
- Choi, S. Y.; Mamak, M.; Coombs, N.; Chopra, N.; Ozin, G. A. *Nano Lett.* **2004**, *4*, 1231.
- Hu, Y. S.; Kienle, L.; Guo, Y. G.; Maier, J. *Adv. Mater.* **2006**, *18*, 1421.
- Guo, Y. G.; Hu, Y. S.; Sigle, W.; Maier, J. *Adv. Mater.* **2007**, *19*, 2087.
- Xu, J. W.; Jia, C. H.; Cao, B.; Zhang, W. F. *Electrochim. Acta* **2007**, *52*, 8044.
- Jiang, C. H.; Honma, I.; Kudo, T.; Zhou, H. S. *Electrochim. Solid-State Lett.* **2007**, *10*, A127.
- Armstrong, A.; Armstrong, G.; Canales, J.; Bruce, P. G. *J. Power Sources* **2005**, *146*, 501.
- Do, J. S.; Weng, C. H. *J. Power Sources* **2006**, *159*, 323.
- Maranchi, J. P.; Hepp, A. F.; Kumta, P. N. *Mater. Sci. Eng., B* **2005**, *116*, 327.
- (a) Subramanian, V.; Karki, A.; Gnanasekar, K. I.; Eddy, F. P.; Rambabu, B. *J. Power Sources* **2006**, *159*, 186. (b) Wang, Z. Y.; Li, S. Z.; Chen, G.; Xia, D. G. *Electrochim. Solid-State Lett.* **2007**, *10*, A77. (c) Jiang, C. H.; Wei, M. D.; Qi, Z. M.; Kudo, T.; Honma, I.; Zhou, H. *J. Power Sources* **2007**, *166*, 239.
- (a) Wang, Y.; Cao, G. Z. *Chem. Mater.* **2006**, *18*, 2787. (b) Wang, Y.; Cao, G. Z. *Adv. Mater.*, in press.
- Chen, J.; Wang, S.; Whittingham, W. S. *J. Power Sources* **2007**, *174*, 442.
- Sides, C. R.; Li, N. C.; Patrissi, C. J.; Scrosati, B.; Martin, C. R. *MRS Bull.* **2002**, *27*, 604.
- Zhou, Y. K.; Cao, L.; Zhang, F. B.; He, B. L.; Li, H. L. *J. Electrochem. Soc.* **2003**, *150*, A1246.
- Wang, Q.; Wen, Z. H.; Li, J. H. *Inorg. Chem.* **2006**, *45*, 6944.
- Zhang, H.; Li, G. R.; An, L. P.; Yan, T. Y.; Gao, X. P.; Zhu, H. Y. *J. Phys. Chem. C* **2007**, *111*, 6143.
- Xiao, P.; Garcia, B. B.; Guo, Q.; Liu, D. W.; Cao, G. Z. *Electrochem. Commun.* **2007**, *9*, 2441.
- Ghico, A.; Tsuchiya, H.; Macak, J.; Schmuki, P. *Phys. Status Solidi A* **2006**, *203*, R28-R30.
- Fattakhova, D.; Kavan, L.; Krtil, P. *J. Solid-State Electrochem.* **2001**, *5*, 196.
- Li, J. R.; Tang, Z. L.; Zhang, Z. T. *Electrochem. Commun.* **2005**, *7*, 62.
- Furukawa, H.; Hibino, M.; Honma, I. *J. Electrochem. Soc.* **2004**, *151*, A527.

- (28) Kim, D. H.; Ryu, H. W.; Moon, J. H.; Kim, J. *J. Power Sources* **2006**, *163*, 196.
- (29) Gao, J.; Zhang, H. P.; Fu, L. J.; Zhang, T.; Wu, Y. P.; Takamura, T.; Wu, H. Q.; Holze, R. *Electrochim. Acta* **2007**, *53*, 1380.
- (30) Yamaguchi, K.; Suzuki, J.; Saito, M.; Sekine, K.; Takamura, T. *J. Power Sources* **2001**, *97–98*, 159.
- (31) Xiao, P.; Liu, D. W.; Garcia, B. B.; Guo, Q.; Sepehri, S.; Cao, G. Z. Unpublished work, 2008.
- (32) Lee, K.; Wang, Y.; Cao, G. Z. *J. Phys. Chem. B* **2005**, *109*, 16700.
- (33) Wang, Y.; Takahashi, K.; Cao, G. Z. *Adv. Funct. Mater.* **2006**, *16*, 1133.

- (34) Wagemaker, M.; Borghols, W.; Mulder, F. *J. Am. Chem. Soc.* **2007**, *129*, 4323.
- (35) Wagemaker, M.; Broghols, W.; van Eck, E.; Kentgens, A.; Kearley, G.; Mulder, F. *Chem. Eur. J.* **2007**, *13*, 2023.
- (36) Ohzuku, T.; Takehara, Z.; Yoshizawa, S. *Electrochim. Acta* **1979**, *24*, 219.
- (37) Kavan, L.; Fattakhova, D.; Krtíl, P. *J. Electrochem. Soc.* **1999**, *146*, 1375.

JP801300J